

A giant radio halo in the cool core cluster CL1821+643

A. Bonafede,¹★ H. T. Intema,² M. Brüggen,¹ H. R. Russell,³ G. Ogrean,¹ K. Basu,⁴
M. Sommer,⁴ R. J. van Weeren,⁵ R. Cassano,⁶ A. C. Fabian³ and H. J. A. Röttgering⁷

¹Hamburger Sternwarte, Universität Hamburg, Gojenbergsweg 112, D-21029 Hamburg, Germany

²National Radio Astronomy Observatory, 1003 Lopezville Road, Socorro, NM 87801-0387, USA

³Institute of Astronomy, Madingley Road, Cambridge CB3 0HA, UK

⁴Argelander Institut für Astronomie, Universität Bonn, D-53121 Bonn, Germany

⁵Harvard–Smithsonian Center for Astrophysics, 60 Garden Street, Cambridge, MA 02138, USA

⁶Istituto di Radioastronomia INAF, via P. Gobetti 101, I-40129 Bologna, Italy

⁷Leiden Observatory, Leiden University, NL-2300 RA Leiden, the Netherlands

Accepted 2014 July 7. Received 2014 July 2; in original form 2014 June 3

ABSTRACT

Giant radio haloes are Mpc-size sources found in some merging galaxy clusters. The synchrotron emitting electrons are thought to be (re)accelerated by plasma turbulence induced by the merging of two massive clusters. Cool core galaxy clusters have a low-temperature core, likely an indication that a major merger has not recently occurred. CL1821+643 is one of the strongest cool core clusters known so far. Surprisingly, we detect a giant radio halo with a largest linear size of ~ 1.1 Mpc. We discuss the radio and X-ray properties of the cluster in the framework of the proposed models for giant radio haloes. If a merger is causing the radio emission, despite the presence of a cool core, we suggest that it should be off-axis, or in an early phase, or a minor one.

Key words: acceleration of particles – radiation mechanism: non – thermal – methods: observational – galaxies: clusters: individual: CL1821+643 PSZ1 G094.00+274 – galaxies: clusters: intracluster medium – radio continuum: general.

1 INTRODUCTION

Giant radio haloes are extended synchrotron sources found in a fraction of massive galaxy clusters. Their surface brightness is faint ($\sim 1 \mu\text{Jy arcsec}^{-2}$ at 1.4 GHz) and characterized by a steep spectrum¹ with a spectral index $\alpha > 1$ (see Feretti et al. 2012 for a recent review). Radio emission on Mpc scales requires that the emitting electrons are either (re)accelerated *in situ*, e.g. through merger-generated turbulence, or continuously injected into the intracluster medium (ICM), for instance by inelastic hadronic collisions between relativistic and thermal protons (see review by Brunetti & Jones 2014, and references therein). Hadronic models are currently disfavoured as they fail to reproduce the steepest spectrum radio haloes, and predict γ -ray emission that has not been observed by the *Fermi* satellite (e.g. Brunetti et al. 2012). At the same time, recent LOw Frequency ARray (LOFAR) observations of Abell 2256 indicate that the formation process of haloes might be more complex than previously thought (van Weeren et al. 2012).

Mini haloes are another class of radio sources that are located in cool core galaxy clusters. Their emission is limited to smaller spatial scales (~ 50 – 500 kpc), and has a steep spectrum (see Feretti

et al. 2012, and references therein). Again, the radio emission could be caused by turbulence induced by gas sloshing in the central potential well or by inelastic collisions between relativistic and thermal protons (e.g. Brunetti & Jones 2014, and references therein).

The picture that emerges from X-ray observations is that mergers between clusters are able to destroy the cool core and leave clear signatures in the emission of the gas (e.g. Rossetti & Molendi 2010). Hence, mergers would be responsible for the cool core–non-cool core dichotomy, supporting an evolutionary scenario between cool core and non-cool core clusters (Rossetti et al. 2011). However, simulations show that disrupting the cool core during cluster mergers is not obvious (see e.g. Poole et al. 2008).

Since their first discovery, giant radio haloes have always been found in merging galaxy clusters, characterized by the absence of a cool core, while mini haloes are found in clusters hosting a cool core (Feretti et al. 2012, and references therein).

The cluster CL1821+643 surrounds the quasar H1821+643. CL1821+643 was discovered by Schneider et al. (1992) through optical observations. The redshift information, available for six member galaxies plus the quasar, allowed them to estimate the cluster redshift: $z = 0.299$. CL1821+643 was also detected by the *Planck* satellite (PSZ1 G094.00+27.41). Through the thermal Sunyaev–Zel’dovich (SZ) effect, Planck Collaboration (2013) infer a mass $M_{500} = 6.311 \times 10^{14} M_{\odot}$. Russell et al. (2010) observed the cluster with *Chandra*. Thanks to an accurate modelling of the quasar

*E-mail: annalisa.bonafede@hs.uni-hamburg.de

¹ The radio spectrum is defined as $S(\nu) \propto \nu^{-\alpha}$.

Table 1. Radio observations of CL1821+643. Column 1: right ascension and declination of the pointing centre if the observation; column 2: date of observation; column 3: central frequency; column 4: bandwidth; column 5: net on-source time; column 6: restoring beam of the full-resolution image; column 7: rms noise of the full-resolution image; column 8: restoring beam of the high-resolution image; column 9: rms noise of the high-resolution image; column 10: restoring beam of the low-resolution image; column 11: rms noise of the low-resolution image.

Pointing RA and Dec. J2000	Obs. date	ν (MHz)	$\Delta\nu$ (MHz)	t (h)	θ_{FR} (arcsec \times arcsec)	σ_{FR} (mJy beam $^{-1}$)	θ_{HR} (arcsec \times arcsec)	σ_{HR} (mJy beam $^{-1}$)	θ_{LR} (arcsec \times arcsec)	σ_{LR} (mJy beam $^{-1}$)
18 21 57.3+64 20 36	27-01-2013	323	33	6	12 \times 9	0.07	11 \times 7	0.13	30 \times 26	0.20
18 21 57.2+64 20 36	22-09-1996	1665	50	0.37	49 \times 32	0.10	45 \times 30	0.16	53 \times 38	0.20

emission, they were able to separate the cluster and quasar emission, and analysed both the ICM properties down to the inner regions, and the interaction of the cluster with the powerful quasar. They found that the temperature of the cluster decreases from ~ 9 to 1.3 keV at the centre, and derived a short radiative cooling time of ~ 1 Gyr, typical of strong cool core systems. In the inner 100 kpc, the X-ray morphology shows extended spurs of emission from the core, a small radio cavity, and a weak shock or cold front at 15 arcsec from the cluster centre. The optical quasar hosts a Fanaroff–Riley type I (FR I) radio source, which is not clearly related to the X-ray gas morphology (Russell et al. 2010).

Wold et al. (2002) have analysed the weak lensing properties of the cluster, finding that the cluster is slightly elongated towards north-west (NW), as also suggested by the X-ray emission on large scales (Russell et al. 2010).

In this work, we present new radio observations of CL1821+643, where we discover diffuse radio emission on Mpc scales. In Section 2, we present Giant Metrewave Radio Telescope (GMRT) and archival Very Large Array (VLA) observations of the cluster. Results are presented in Section 3, where we also analyse the dynamical status of the cluster. We discuss the results and conclude in Section 4. Throughout this Letter, we assume a Λ cold dark matter cosmology ($H_0 = 71 \text{ km s}^{-1} \text{ Mpc}^{-1}$, $\Omega_m = 0.27$, $\Omega_\Lambda = 0.73$). At the cluster redshift ($z = 0.299$), 1 arcmin corresponds to 265 kpc.

2 RADIO OBSERVATIONS

We have observed the cluster CL1821+643 with the GMRT in the framework of a larger project aimed at discovering diffuse emission in clusters detected by *Planck*. Observations were carried out at 323 MHz, using a 33 MHz bandwidth subdivided into 256 channels and 8 s integration time. The sources 3C48 and 3C286 were observed for 15 min at the beginning of the observing block, and used as absolute flux and bandpass calibrators, adopting the Scaife & Heald (2012) absolute flux scale. The absolute flux calibrators were also used to estimate the instrumental contribution to the antenna gains, which is also needed for ionospheric calibration, and the instrumental phase information was used to correct the target field. The main steps of the calibration procedure are outlined below, and are based on AIPS (National Radio Astronomy Observatory Astronomical Image Processing System), SPAM (Intema et al. 2009), and OBIT (Cotton 2008) tools. Strong radio frequency interferences (RFIs) were removed from the target field data by statistical outlier flagging tools. Remaining low-level RFIs were modelled and subtracted from the data using OBIT. The data set has been averaged down to 24 channels, a compromise to speed up the imaging process and avoid significant bandwidth smearing. For the phase calibration, we started from a model derived from the NRAO VLA Sky Survey (Condon et al. 1998) and then proceeded with self-calibration loops. To compensate for the non-coplanarity of the array, we used the polyhedron (facet-based) wide-field imaging technique as available in AIPS. We performed several rounds of

imaging and self-calibration, inspecting the residual visibilities for a more accurate removal of low-level RFIs. To correct for ionospheric effects, we applied SPAM calibration and imaging. The presence of strong sources in the field of view enables one to derive directional-dependent gains for each of them and to use these gains to fit a time-variable phase screen over the entire array. After ionospheric corrections, data have been imported to CASA (Common Astronomy Software Applications package) for further imaging and self-calibration steps.

In addition, we have downloaded an observation performed in the L band in the D array configuration from the VLA data archive. Using AIPS, we followed a standard procedure for the data reduction. The source 3C286 has been used to set the absolute flux, using the Perley & Taylor (1999) flux scale. As no phase calibrator was scheduled during the observation, we transferred the gains from 3C286 to the target and proceeded with cycles of self-calibration on the target field. Details about the observation are listed in Table 1.

For both GMRT and VLA observations, we have produced three different images of the target field.

- (i) Full-resolution (FR) image: using all the baselines and Briggs weighting scheme with robust $R = 0$.
- (ii) High-resolution (HR) image: using all the baselines longer than $0.9k\lambda$, to filter out the emission on scales larger than 1 Mpc. Sources have been cleaned down to 1σ , σ being the rms noise level of the image. On these images, we have identified the sources within a radius of 1 Mpc from the cluster centre (see Fig. 1). The quasar

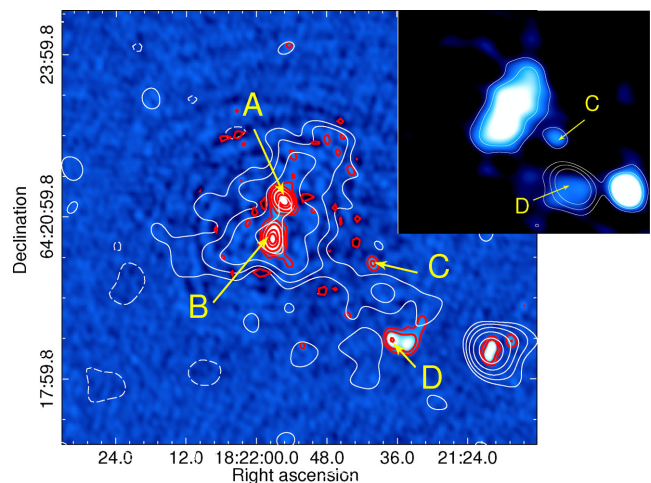


Figure 1. The cluster CL1821+643. Main panel – colours and red contours: HR image at 323 MHz. White contours: LR image at 323 MHz. The first contours are drawn at $3\sigma_{\text{LR,HR}}$, and other contours are spaced by a factor 2. The $-3\sigma_{\text{LR,HR}}$ contours are dashed. In the inset: LR image at 1665 MHz in colours and contours (at 3, 6, $12\sigma_{\text{LR}}$, the $-3\sigma_{\text{LR}}$ contour is dashed). The inset shows the same region as the main panel (A and B have been subtracted).

and the head–tail radio galaxy detected by Blundell & Rawlings (2001) are labelled as B and A, respectively.

(iii) Low-resolution (LR) image: first, we subtracted from the uv -data the visibilities corresponding to the clean components of the HR image for the sources A, B, C, and D (see Fig. 1). Then, we imaged the uv -subtracted data set including all baselines and tapering down the baselines longer than $4k\lambda$ to gain sensitivity towards the diffuse emission.

The final images were corrected for the primary beam response. Furthermore, GMRT images have been corrected for the system temperature using the Haslam et al. (1995) all-sky map. We estimate that the residual amplitude errors are of the order of 6 per cent at 323 MHz. VLA observations amplitude errors are ~ 4 per cent at 1.665 GHz.

3 RESULTS

3.1 Radio emission and cluster properties

As shown in Fig. 2, diffuse radio emission is clearly detected in CL1821+643. We note that other compact sources, which we subtracted from the uv -data, do not leave residuals in the LR images. To analyse its radio morphology, we rely on the 323 MHz observation, which has a longer exposure time and a wider range of baselines with respect to the 1.665 GHz one. In Fig. 2, the LR image at 323 MHz is shown. The radio emission is located at the cluster centre, and extends for ~ 1 Mpc towards NW. Because of its size and location, we classify this emission as a giant radio halo.

Further emission is tentatively detected at 3σ significance at the west of the cluster (see Fig. 2). Although it does not overlap with sources C and D (Fig. 1), deeper observations would be needed to confirm the detection. We have measured the flux density of the giant radio halo on the LR images at 323 MHz and at 1.665 GHz. The error on the giant radio halo flux has been estimated as $\Delta S = \sqrt{(F_h \text{Err}_{\text{cal}})^2 + (\sigma_{\text{LR}} \sqrt{N_b})^2}$, where F_h is the flux density of the giant radio halo measured from the LR image, Err_{cal} is the calibration error, σ_{LR} is the rms noise of the LR image, and N_b is

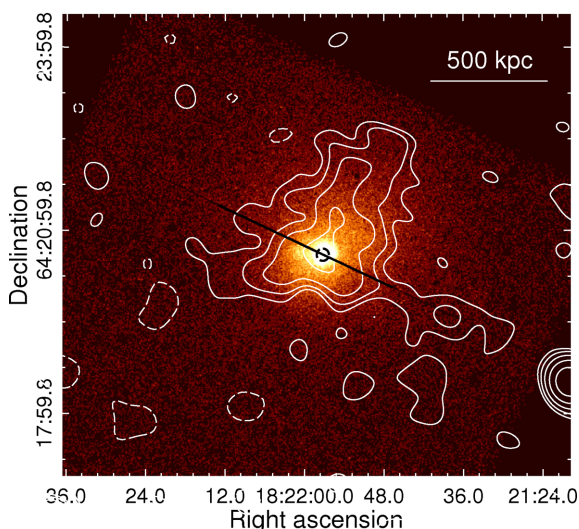


Figure 2. Colours: *Chandra* exposure-corrected image in the 0.5–7 keV energy band smoothed with a 2D Gaussian of $\sigma = 1$ arcsec. The readout strip is blanked. Contours are the same as the 323 MHz LR image in Fig. 1. The black dashed circle is centred on the quasar and has a radius of $0.05 \times R_{\text{ap}}$ (see the text for details).

Table 2. Properties of the giant radio halo.

Frequency (MHz)	Flux density (mJy)	Largest angular scale (arcsec)	Largest linear scale (kpc)
323	62 ± 4	250	1100
1665	11.9 ± 0.5	210	930

the number of independent beams sampling the diffuse emission. Details about the giant radio halo flux density and size are listed in Table 2.

To estimate the spectral index of the halo, we imaged the uv -subtracted data, selecting the range of baselines that are densely sampled by both observations (from 0.3 to 5.5 $k\lambda$) and convolved the images with the same beam of ~ 60 arcsec \times 50 arcsec. Because of the poorer sensitivity of the 1.665 GHz observation, only the central region is detected. It has a spectral index of $\alpha = 0.87 \pm 0.04$. Using these images, a lower limit for the spectral index of the entire halo can be derived, computing the flux densities in both images wherever the 323 MHz image has a signal above three times the noise level, obtaining $\alpha \geq 1.04$. Using the fluxes measured in the LR images at 323 MHz and 1.665 GHz (Table 2), we obtain an upper limit for the spectral index: $\alpha \leq 1.1$.

The power of giant radio haloes is known to correlate with the cluster X-ray luminosity: $P_{1.4\text{GHz}} - L_{[0.1-2.4]\text{keV}}$ correlation, and with the cluster SZ signal: $\text{SZ} - P_{1.4\text{GHz}}$ correlation (Basu 2012; Cassano et al. 2013). We have computed the power of the giant radio halo at 1.4 GHz extrapolating the flux density observed in the 323 MHz image and assuming a spectral index in the range $1.04 \leq \alpha \leq 1.1$. The estimated power at 1.4 GHz, $P_{1.4\text{GHz}}$, is in the range $(3.6-3.8) \times 10^{24}$ W Hz $^{-1}$. We have computed $L_{[0.1-2.4]\text{keV}}$ from the *Chandra* observation of the cluster presented in Russell et al. (2010), using an absorbed MEKAL model in the X-ray fitting package XSPEC with a temperature $T = 7.0 \pm 0.2$ keV and a metallicity $Z = (0.29 \pm 0.03) Z_{\odot}$. We obtain $L_{[0.1-2.4]\text{keV}} = (1.44 \pm 0.01) \times 10^{45}$ erg s $^{-1}$, which would put the halo a factor of ~ 3 below the $P_{1.4\text{GHz}} - L_{[0.1-2.4]\text{keV}}$ correlation, i.e. the cluster is underluminous in radio for its X-ray luminosity. $L_{[0.1-2.4]\text{keV}}$ is here computed within an aperture of 650 kpc, the maximum allowed by this *Chandra* observation, while Cassano et al. (2013) computed $L_{[0.1-2.4]\text{keV}}$ within r_{500} , corresponding to ~ 1.2 Mpc for this cluster. Hence, the cluster could be more than a factor of 3 below the correlation. The SZ flux is a more robust estimate of the cluster mass, since it is less biased by the dynamical state of the cluster. Indeed, the cluster follows the $\text{SZ} - P_{1.4\text{GHz}}$ correlation within the errors.

3.2 Characterization of the dynamical state

Since radio haloes are always found in merging galaxy clusters, it is crucial to characterize the dynamical status of CL1821+643. To this aim, we compute three dynamical indicators, extensively used in the literature (e.g. Böhringer et al. 2010): the power ratio P_3/P_0 , the centroid shift w , and the concentration parameter c . Recently, Cassano et al. (2010) have used these methods, finding that clusters with and without radio haloes occupy different regions in the morphological diagrams (see Fig. 3), and confirming that radio haloes are always associated with merging clusters.

The *Chandra* image of the cluster CL1821+643 has been exposure, vignetting, and background corrected, and the quasar emission has been subtracted. P_3/P_0 , w , and c have been computed within an aperture radius $R_{\text{ap}} = 500$ kpc. Because of the quasar and of the readout strip, the centre of the cluster, used in the following

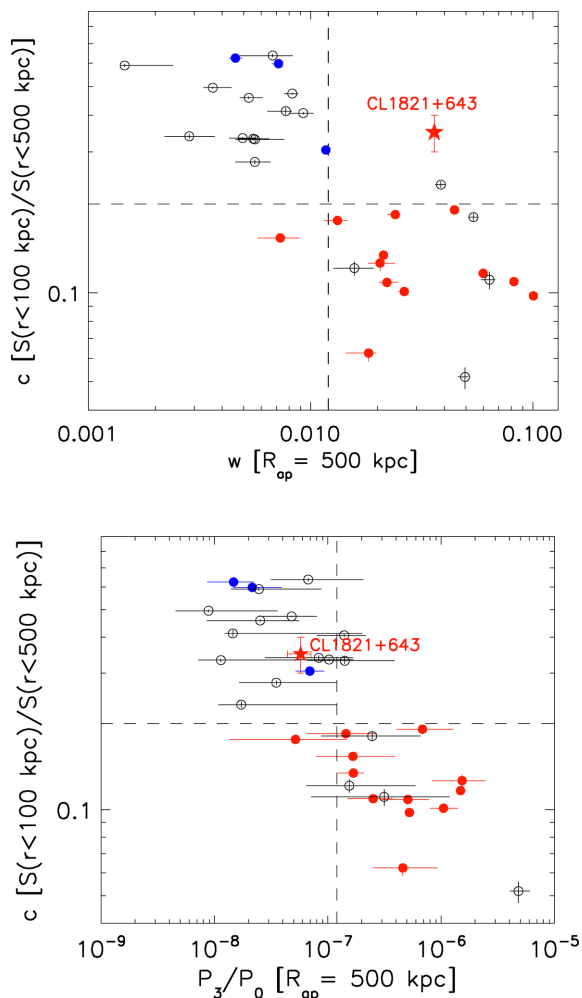


Figure 3. The $c-w$ (top panel) and $c-P_3/P_0$ (bottom panel) diagrams. The red star marks the position of CL1821+643. Dashed lines are the median of the parameters, which define the radio-loud and radio-quiet quadrants, red dots mark giant radio haloes, blue dots mark mini haloes, and black circles mark radio-quiet clusters (points and lines are taken from Cassano et al. 2010).

analysis, is not uniquely defined. We consider as centre the position of the quasar.² The errors and the photon bias have been estimated through Monte Carlo simulations, following the approach of Böhringer et al. (2010).

The power ratio is a multipole decomposition of the two-dimensional projected mass distribution (Buote & Tsai 1995). We have determined the power ratio P_3/P_0 , the lowest power ratio moment providing a clear substructure measure, obtaining $P_3/P_0 = (5.8 \pm 1.4) \times 10^{-8}$. Since the momenta are computed excising the inner $0.05 \times R_{\text{ap}}$, the quasar does not affect the P_3/P_0 computation.

The centroid shift method (Maughan et al. 2008) measures the standard deviation of the projected separation between the X-ray peak and the centroid in units of R_{ap} , computed within circles of

increasing radius (from $0.05 \times R_{\text{ap}}$ to R_{ap} , in steps of $0.05 \times R_{\text{ap}}$). The centroid shift, w , has been computed minimizing the P_1 dipole within circles of increasing radius (as done by Böhringer et al. 2010) and computing the X-ray weighted centroid (following Cassano et al. 2010). We obtain $w = (5.98 \pm 0.07) \times 10^{-2}$ and $(3.6 \pm 0.07) \times 10^{-2}$, respectively.

The concentration parameter, c , measures the ratio between the X-ray surface brightness within 100 kpc and the surface brightness within 500 kpc. Because of the quasar and the readout strip, we can only derive limits for c , with and without the quasar subtraction. We obtain $0.3 < c < 0.4$.

In Fig. 3, we show the position of the cluster in the P_3/P_0-c and $w-c$ diagrams, taken from Cassano et al. (2010). In the P_3/P_0-c diagram, the cluster is among the radio-quiet ones. The w parameter, instead, has a typical value for clusters with a giant radio halo, i.e. dynamically disturbed. Hence, in the $c-w$ and $w-P_3/P_0$ diagrams (not shown here), the cluster is in a rather empty quadrant.

4 DISCUSSION AND CONCLUSIONS

A giant radio halo in a cool core cluster challenges our understanding of cool core clusters, major mergers, and radio emission. So far, giant radio haloes have always been found in massive mergers, and never in cool core clusters, hence supporting the idea that major mergers, necessary to power giant radio haloes, also disrupt the cool core. In this framework, few peculiar cases have been found: RX J1347.5–1145, which shows both a cool core and merging signatures, and hosts a mini halo (Gitti et al. 2007), and A2142, where the cool core has been destroyed by the merger, but some remnants seem to be sloshing, and a giant radio halo has been detected (Farnsworth et al. 2013). CL1821+643 is the only case found so far where a giant radio halo is detected in a cluster that preserves the cool core.

So far, giant radio haloes and mini haloes have been considered as two separate classes of sources. CL1821+643 could be witnessing the transition between these two stages: turbulent motions generated during mergers could switch off the mini halo and transport relativistic electrons on larger scales (Brunetti & Jones 2014). In this case, one should assume that a merger is taking place here, and that it has not disrupted the cool core.

The X-ray observations indicate that the cluster is not undergoing a major merger similar to those detected in other clusters with radio haloes. However, it could be undergoing a minor or off-axis merger, which may be responsible for the high value of the centroid shift w and the possible sloshing structure (Russell et al. 2010). As none of the morphological indicators is sensitive to mergers along the line of sight, spectroscopic observations are needed to finally assess the dynamical status of CL1821+643. The analysis of the X-ray substructure highlights the peculiarities of CL1821+643, even without the radio information. Indeed, it shows features typical of systems in dynamical equilibrium (cool core, temperature and entropy drop, high value of the concentration parameter c) as well as indication of large-scale perturbations (high value of the centroid shift w and sloshing).

Another possibility is that the radio emission is not a radio halo but a radio relic seen in projection. Radio relics could be originated by minor off-axis mergers that preserve the cool core, like in Abell 1664 (Govoni et al. 2001). However, the presence of a radio relic seen in projection on to the cluster centre is unlikely (Vazza et al. 2012) and neither the morphology of the emission nor the NW elongation – roughly following the X-ray emission – would favour this interpretation.

² We repeated the calculations assuming different centres: (i) the pixel that provides the minimum value of the dipole P_1 , (ii) the X-ray centroid, and (iii) the position where the X-ray emission is maximum. All these choices are affected by the quasar excision and, as such, less reliable. None the less, the results we obtain differ by few per cent.

Finally, the extended emission could result from the past activity of an FR II radio source, now turned into the FR I associated with the quasar, hence not requiring a merger to accelerate the particles. We regard this possibility as less plausible because of the relatively low α and the morphology of the radio emission. However, spectral index maps would be needed to investigate this scenario.

To conclude, our results can be summarized as follows.

(i) We have analysed the radio emission of the cluster CL1821+643 – also known as PSZ1 G094.00+27.41 – finding for the first time a strong cool core cluster that hosts a giant radio halo, having a largest linear scale of ~ 1.1 Mpc.

(ii) We have constrained the spectral index between 323 MHz and 1.665 GHz to be $1.04 \leq \alpha \leq 1.1$, meaning that the halo is in an early stage of its radio-loud phase.

(iii) The radio power at 1.4 GHz is at least a factor of ~ 3 below the $P_{1.4\text{GHz}} - L_{[0.1-2.4]\text{keV}}$ correlation, while it sits on the $SZ - P_{1.4\text{GHz}}$ correlation.

(iv) An analysis of the cluster, based on the X-ray P_3/P_0 and c morphological estimators, would classify the cluster among the radio-quiet systems. However, the high value of w indicates that some merger has happened here.

If the radio emission is powered by merger-induced turbulence, we have to assume that the cluster is undergoing a merger which has not disrupted the cool core, but has injected a sufficient amount of energy to power the radio emission. In re-acceleration scenarios, this suggests that a higher fraction of the gravitational energy, released into the ICM during mergers, might be channelled into the (re)acceleration of particles, or that a seed population of energetic particles is already present.

ACKNOWLEDGEMENTS

We thank F. de Gasperin and F. Vazza for useful discussions. AB and MB acknowledge support by the research group FOR 1254 funded by the Deutsche Forschungsgemeinschaft. HR acknowledges support from ERC Advanced Grant Feedback. RJW is supported by NASA through Einstein Postdoctoral grant PF2-130104 (Chandra X-ray Center, SAO for NASA, contract NAS8-03060). We also thank the staff of the GMRT. NRAO is a facility of the National Science Foundation operated under Associated Universities Inc.

REFERENCES

- Basu K., 2012, MNRAS, 421, L112
 Blundell K. M., Rawlings S., 2001, ApJ, 562, L5
 Böhringer H. et al., 2010, A&A, 514, A32
 Brunetti G., Jones T. W., 2014, Int. J. Modern Phys. D, 23, 30007
 Brunetti G., Blasi P., Reimer O., Rudnick L., Bonafede A., Brown S., 2012, MNRAS, 426, 956
 Buote D. A., Tsai J. C., 1995, ApJ, 452, 522
 Cassano R., Ettori S., Giacintucci S., Brunetti G., Markevitch M., Venturi T., Gitti M., 2010, ApJ, 721, L82
 Cassano R. et al., 2013, ApJ, 777, L41
 Condon J. J., Cotton W. D., Greisen E. W., Yin Q. F., Perley R. A., Taylor G. B., Broderick J. J., 1998, AJ, 115, 1693
 Cotton W. D., 2008, PASP, 120, 439
 Farnsworth D., Rudnick L., Brown S., Brunetti G., 2013, ApJ, 779, 189
 Feretti L., Giovannini G., Govoni F., Murgia M., 2012, A&AR, 20, 54
 Gitti M., Ferrari C., Domainko W., Feretti L., Schindler S., 2007, A&A, 470, L25
 Govoni F., Feretti L., Giovannini G., Böhringer H., Reiprich T. H., Murgia M., 2001, A&A, 376, 803
 Haslam C. G. T., Salter C. J., Stoffel H., Wilson W. E., 1995, Astronomy Data Image Library, p. 1
 Intema H. T., van der Tol S., Cotton W. D., Cohen A. S., van Bemmell I. M., Röttgering H. J. A., 2009, A&A, 501, 1185
 Maughan B. J., Jones C., Forman W., Van Speybroeck L., 2008, ApJS, 174, 117
 Perley R. T., Taylor G. B., 1999, VLA Calibrator Manual, Technical report, NRAO, Charlottesville, VA
 Planck Collaboration, 2013, A&A, preprint (arXiv:1303.5089)
 Poole G. B., Babul A., McCarthy I. G., Sanderson A. J. R., Fardal M. A., 2008, MNRAS, 391, 1163
 Rossetti M., Molendi S., 2010, A&A, 510, A83
 Rossetti M., Eckert D., Cavalleri B. M., Molendi S., Gastaldello F., Ghizzardi S., 2011, A&A, 532, A123
 Russell H. R., Fabian A. C., Sanders J. S., Johnstone R. M., Blundell K. M., Brandt W. N., Crawford C. S., 2010, MNRAS, 402, 1561
 Scaife A. M. M., Heald G. H., 2012, MNRAS, 423, L30
 Schneider D. P., Bahcall J. N., Gunn J. E., Dressler A., 1992, AJ, 103, 1047
 van Weeren R. J. et al., 2012, A&A, 543, A43
 Vazza F., Brüggem M., van Weeren R., Bonafede A., Dolag K., Brunetti G., 2012, MNRAS, 421, 1868
 Wold M., Lacy M., Dahle H., Lilje P. B., Ridgway S. E., 2002, MNRAS, 335, 1017

This paper has been typeset from a $\text{\TeX}/\text{\LaTeX}$ file prepared by the author.